

Geometric Adaptive Robust Sliding-mode Control on SO(3)

Yulin Wang^a, Xiao Wang^b, Shengjing Tang^c and Jie Guo^d
School of Aerospace and Engineering, Beijing Institute of Technology, Beijing, China

Keywords: Geometric Attitude Control, SO(3), Adaptive Robust Control, Sliding-mode Control.

Abstract: This paper addresses the rigid body attitude tracking control on the manifold SO(3). This modeling scheme can avoid the singularity and ambiguity associated with local parameterization representations such as Euler angles and quaternion. A robust and almost global asymptotic stability control system is designed considering the parameters uncertainty and external interference. Based on the coordinate-free geodesic attitude error scalar function with its deduced attitude and velocity error vectors, a geometric asymptotic convergent sliding-mode surface is designed firstly. Then, a geometric sliding-mode controller is introduced to enhance the robustness of the system for the low-amplitude fast-time-varying disturbances. Moreover, in order to attenuate the effect of the parameters uncertainty and slow-time-varying disturbance, two adaptive functions are employed to obtain the feedforward compensation. Comparison studies and simulation results show that the proposed controller is more practical with a high accuracy, strong robustness, less chattering and simple structure.

1 INTRODUCTION

The movement of a rigid body in a three-dimensional space can be divided into the movement in translational space and the movement in rotational space. The rotation control is usually the basis of the translation control for most rigid bodies. For example, in astronautics, the control forces of the satellite or missile are mainly produced by the thrusters. In aeronautics, the control forces of the aircraft or quadrotor are mainly produced by their wings and propellers. They are all executed based on the maneuver of a rigid body's orientation and rotation. Therefore, the rigid-body attitude control has been studied and applied extensively in many areas recently, such as aerial vehicles, spacecraft vehicles, underwater vehicles, ground vehicles, and robotics (Islam et al., 2017; Forbes, 2014; Zlotnik and Forbes, 2014).

The orientation of the rigid body in a three-dimensional space can be uniquely described by a directional cosine matrix, which is the element of the Lie group SO(3) (three-dimensional special

orthogonal group). SO(3) is also a nonlinear differentiable manifold with nine elements and six constraints. It is hard to analyze the geometric and algebra properties of SO(3) using the method in Euclidean space, which will be detailed later. Therefore, local parameterizations of SO(3) were mainly studied historically. However, all minimal parameter presentations, such as Euler angle, Rodrigues parameters and modified Rodrigues parameters, are local and suffer from singularities. Quaternions consisting of four parameters do not have singularities but have ambiguities. It suffers from the unwinding phenomena. Because the three-dimensional sphere S^3 double covers SO(3). In order to avoid the singularities and ambiguities in representing an attitude, the controllers using SO(3) directly in a coordinate-free format have been developed in recent years (Lee, Leoky and McClamroch, 2011; Liu et al., 2016; Maithripala and Berg, 2015).

The early results of nonlinear differentiable manifolds are studied in (Boothby, 2003), where the

^a <https://orcid.org/0000-0003-2666-836X>

^b <https://orcid.org/0000-0002-7583-7628>

^c <https://orcid.org/0000-0003-4224-9579>

^d <https://orcid.org/0000-0003-0951-5126>

differential and integration properties, the tensor and tensor field on Riemannian manifolds are derived. Koditschek (Koditschek, 1988) designed the PD based controller on SO(3), where the almost globally asymptotically stability of the closed-loop system is proved. Bullo (Bullo and Murray, 1999) proposed a unified framework to design the controller for the mechanical systems modeled on nonlinear manifolds, such as \mathbb{S}^2 , SO(3) and SE(3). For SO(3), it is also a Lie group with its compatible group operation and zero element. Using the left-invariant property of Lie group, the attitude and velocity error vectors can be translated into its Lie algebra space, which is diffeomorphism to \mathbb{R}^3 (Bullo and Murray, 1995; Bullo and Murray, 1999; Maithripala and Berg, 2015). Then, the vector operations addition and subtraction can be used again in this case. Employing these properties, Lee (Taeyoung, 2012; Lee, 2012; Lee, 2008) designed some specific attitude error scalar functions on SO(3), and based on these attitude error scalar functions, the matching attitude controllers are designed.

However, the existing attitude controllers on SO(3) are almost all designed based on the standard augmented PD control with a feedforward compensation loop (Bullo and Lewis, 2005; Lee, 2008; Lee et al., 2011). Besides, all those control laws are designed based on the assumptions that the model is precisely modeled in advance and there is no external disturbance. The controllers above for a perfect attitude tracking can not be realized in practice due to the ideal assumptions. One feasible way to solve this problem is designing an adaptive robust controller (ARC) to estimate the uncertain inertial matrix and constant external disturbances (Fernando et al., 2011; Sanyal et al., 2009). However, these adaptive controllers do not consider the time-varying disturbances. The sliding-mode controller (SMC) can deal with all bounded disturbances (Liu et al., 2016). However, SMC will cause a heavy chattering phenomenon for the high-amplitude disturbances, which might be dangerous in practice.

Combined with the virtues of ARC and SMC, the adaptive robust sliding-mode controller (ARSMC) can handle these problems efficiently (Islam et al., 2017). However, the ARSMC is hard to apply to a nonlinear manifold and its tangent space. As the attitude error vector of nonlinear manifold is deduced from the error scalar function (Bullo and Murray, 1999). The error dynamics of nonlinear manifolds are not only determined by the topology structure of the manifold generally, but also related to the choice of the error scalar function. For the closed compact

manifolds which are not diffeomorphism to any Euclid space, such as these familiar nonlinear manifolds \mathbb{S}^2 , \mathbb{S}^3 , SO(3) and SE(3), the magnitude of the attitude error vector designed in (Bullo and Murray, 1999; Bullo and Lewis, 2005) will decrease to zero at each isolated critical points. Therefore, the conventional design process of the asymptotically convergent sliding-mode surface, which will let the attitude error vector converge to zero, are infeasible. Moreover, the time derivative of the attitude error vector is not equal to and even not positively related to the velocity error vector. The relationship between these two error vectors is often ambiguous which is determined by the choice of the attitude error scalar function. For SO(3), the time derivative of the attitude error vector can be expressed as a three-dimensional intermediate variable matrix $E \in \mathbb{R}^{3 \times 3}$ multiplies the velocity error vector (Lee, 2012). However, the eigenvalues of the matrix E may be indefinite, which are also determined by the choice of the error scalar function. All those properties above lead to the failure of the methods used in Euclid space. Therefore, The ARSMC has never been applied to the attitude control of a rigid body modeled on SO(3).

Following the geometric control approaches of the prior arts, a geometric adaptive robust sliding-mode controller (GARSMC) on SO(3) is designed in this paper. The geometric asymptotically convergent sliding-mode surface is designed firstly, where the geometric properties of the error scalar function proposed in (Lee, 2012) and its deduced attitude and velocity error vectors are applied. Moreover, an exponential reaching law is adopted to stabilize the closed-loop system. In order to facilitate the controller design, the unknown external disturbance torque in the body-fixed frame is divided into the high-amplitude slow-time-varying part and the low-amplitude fast-time-varying part. Then, the adaptive functions for the uncertain inertial matrix and the unknown high-amplitude slow-time-varying disturbances are designed, respectively. Moreover, the low-amplitude high-frequency disturbances, which can not be estimated rapidly by the adaption function, can be dealt with by the geometric sliding-mode control (GSMC) part with small switching term amplitudes which can also suppress the undesired chattering.

Compared with the prior ARC in (Fernando et al., 2011; Sanyal et al., 2009), the proposed adaptive controller part has a simpler structure with less computation costs. Compared with the prior SMC in (Liu et al., 2016), the proposed controller also has a

simpler sliding-mode surface and less chattering. Besides, the proposed controller can be used to handle a more general class of unconstructed and non-harmonic uncertainties than the prior works (Fernando et al., 2011; Lee, 2012; Liu et al., 2016; Sanyal et al., 2009). Numerical simulations results shows that the proposed controller has a strong anti-interference ability compared with the PD-based controller (Lee, 2012) and ARC, and less chattering phenomenon compared with SMC. The topology structure of compact manifold precludes the existence of a smooth global asymptotic stabilization control (Bhat and Bernstein, 2000). However, using Lyapunov stability theory, the almost global asymptotic stability can be proved for the proposed controller. The convergent region of the unique stable point covers SO(3) but only excludes a set of zero measure critical points. Simulation results illustrate the effectiveness of the proposed controller.

The paper is organized as follows. The attitude dynamic model of a rigid body is developed in section 2. The attitude error scalar function and its deduced attitude error dynamics are analyzed in section 3. The proposed geometric adaptive robust sliding-mode controller is designed in section 4. The numerical simulation follows in section 5. Section 6 summarizes the results and conclusions of this paper.

2 MODELING

The kinematics and dynamics of a rigid body's rotation movement in a three-dimensional Euclidean space are considered in this section. The earth-fixed coordinate is defined as the inertial reference frame, and the body-fixed frame is defined attached to the rigid-body's mass center. The rigid-body attitude kinematics and dynamics equations can be described as (Bullo and Murray, 1995),

$$\begin{cases} \dot{R} = R\Omega^\wedge \\ J\dot{\Omega} + \Omega \times J\Omega = u + d \end{cases} \quad (1)$$

where $\Omega \in \mathbb{R}^3$ is the angular velocity with respect to the body-fixed frame. The rotation matrix $R \in SO(3)$ represents the direction cosine matrix (DCM) from the body-fixed frame to the inertial reference frame. The attitude R of the nonlinear manifold SO(3) satisfies

$$SO(3) = \{R \in \mathbb{R}^{3 \times 3} \mid R^T R = I, \det(R) = 1\} \quad (2)$$

$J \in \mathbb{R}^{3 \times 3}$ is the inertial matrix. $u \in \mathbb{R}^3$ is the

control torque. $d \in \mathbb{R}^3$ is the disturbance defined in the body-fixed frame. It consists of the high-amplitude slow-time-varying disturbances d_0 and the low-amplitude fast-time-varying disturbances d_1 , which satisfies

$$d = d_0 + d_1 \quad (3)$$

d_0 is mainly caused by the deviation of the mass center of the rigid body. d_1 is mainly caused by the unknown friction force, such as the air drag for quadrotor, and randomly external interferences, such as random wind for aircraft. The isomorphism hat map $(\cdot)^\wedge : \mathbb{R}^3 \rightarrow so(3)$ denotes a skew-symmetric matrix operation which can be defined as

$$\Omega^\wedge = \begin{bmatrix} 0 & -\Omega_3 & \Omega_2 \\ \Omega_3 & 0 & -\Omega_1 \\ -\Omega_2 & \Omega_1 & 0 \end{bmatrix} \quad (4)$$

where $so(3)$ is the Lie algebra. The inverse of the hat map is denoted by the vee map $(\cdot)^\vee : so(3) \rightarrow \mathbb{R}^3$.

For any $x, y \in \mathbb{R}^3$, $A \in \mathbb{R}^{3 \times 3}$ and $R \in SO(3)$, it can be proved easily that several properties of the hat map and the vee map are satisfied as follows (Lee, 2012):

$$\begin{aligned} x^\wedge y - x \times y &= -y \times x = -y^\wedge x \\ \text{tr}(Ax^\wedge) &= \frac{1}{2} \text{tr}(x^\wedge(A - A^T)) = -x^T(A - A^T)^\vee \\ x^\wedge A + A^T x^\wedge &= ((\text{tr}(A)I - A)x)^\wedge \\ Rx^\wedge R^T &= (Rx)^\wedge \end{aligned} \quad (5)$$

3 ERROR DYNAMICS

The twice differentiable desired attitude trajectory is denoted by $R_d(t) \in SO(3)$. What we need to do is designing a control law $u \in \mathbb{R}^3$ to track $R_d(t)$, considering the existence of the parameters uncertainties and external disturbance. The kinematics equation of the desired trajectory can be written as

$$\Omega_d^\wedge = R_d^T \dot{R}_d \quad (6)$$

where $\Omega_d \in \mathbb{R}^3$ is the desired angular velocity with respect to the body-fixed frame.

3.1 Assumptions

The following conditions are assumed.

1. The inertial matrix \mathbf{J} of a rigid body is regarded as a constant diagonal matrix, which is

$$\mathbf{J} = \text{diag}(J_1 \ J_2 \ J_3) \quad (7)$$

\mathbf{J} cannot be acquired precisely in advance. However \mathbf{J} is bounded with the known bounds as

$$0 < \mathbf{J}_m \leq \mathbf{J} \leq \mathbf{J}_M \quad (8)$$

where \mathbf{J}_m and \mathbf{J}_M are two known constant diagonal matrix.

2. The slow-time-varying disturbances \mathbf{d}_0 and fast-time-varying disturbances \mathbf{d}_1 are bounded with two known constant array $\mathbf{D}_0 \in \mathbb{R}^3$ and $\mathbf{D}_1 \in \mathbb{R}^3$ respectively as

$$\begin{cases} |\mathbf{d}_0| \leq \mathbf{D}_0 \\ |\mathbf{d}_1| \leq \mathbf{D}_1 \end{cases} \quad (9)$$

3. The desired attitude trajectory is smooth and bounded.

3.2 Attitude Error Dynamics

The topological structures and geometric properties of nonlinear differentiable manifolds are quite different from those of the classical mechanics in Euclidean space (Boothby, 2003; Bhat and Bernstein, 2000). Before the controller is designed, the geometric attitude tracking error and its compatible zero element should be defined firstly. The geometric tracking error between $\mathbf{R}(t)$ and $\mathbf{R}_d(t)$ are defined as $\mathbf{R}_e = \mathbf{R}_d^T \mathbf{R} \in \text{SO}(3)$. The zero element of \mathbf{R}_e is the three-dimensional identity matrix (Bullo and Murray, 1999; Maithripala and Berg, 2015).

For a given attitude tracking command $(\mathbf{R}_d, \boldsymbol{\Omega}_d)$, a smooth geodesic attitude error scalar function $\varphi: \text{SO}(3) \times \text{SO}(3) \rightarrow \mathbb{R}$ is defined as (Lee, 2012)

$$\varphi(t) = \varphi(\mathbf{R}(t), \mathbf{R}_d(t)) = 2 - \sqrt{1 + \text{tr}(\mathbf{R}_d^T \mathbf{R})} \quad (10)$$

It can be proved from (Lee, 2012) that the following properties are satisfied for any \mathbf{R}_d and \mathbf{R} :

- i. $\varphi(\mathbf{R}, \mathbf{R}_d) \geq 0$.
- ii. $\varphi(\mathbf{R}, \mathbf{R}_d) = 0$ if and only if $\mathbf{R}_d = \mathbf{R}$.
- iii. The error scalar function φ is symmetric with $\varphi(\mathbf{R}, \mathbf{R}_d) = \varphi(\mathbf{R}_d, \mathbf{R})$.

The attitude error scalar function φ gets its

unique global minimum $\varphi = 0$ at $\mathbf{R} = \mathbf{R}_d$. It provides a measurement for the magnitude of the tracking error between the two attitudes \mathbf{R} and \mathbf{R}_d to some extent. Except for $\mathbf{R} = \mathbf{R}_d$, the attitude error scalar function φ has some other critical points, which are determined by the topology of $\text{SO}(3)$ and corresponds to the global maximum point of function φ . These isolated critical points are also the local equilibrium points of the closed loop system. Therefore, it is impossible to find a globally stable continuous feedback controller on $\text{SO}(3)$ and only the almost global stability can be achieved for the closed-loop system (Bhat and Bernstein, 2000).

Using the properties in (5), the time derivative of \mathbf{R}_e can be deduced as (Lee, 2012)

$$\frac{d}{dt}(\mathbf{R}_e) = \mathbf{R}_e (\boldsymbol{\Omega} - \mathbf{R}^T \mathbf{R}_d \boldsymbol{\Omega}_d)^\wedge \quad (11)$$

Furthermore, the time derivative of the error scalar function φ can be obtained as

$$\begin{aligned} \frac{d}{dt} \varphi(\mathbf{R}(t), \mathbf{R}_d(t)) = & \\ & \frac{1}{2\sqrt{1 + \text{tr}(\mathbf{R}_d^T \mathbf{R})}} (\mathbf{R}_d^T \mathbf{R} - \mathbf{R}^T \mathbf{R}_d)^\vee \cdot (\boldsymbol{\Omega} - \mathbf{R}^T \mathbf{R}_d \boldsymbol{\Omega}_d) \end{aligned} \quad (12)$$

According to the geometric description of the attitude and velocity error vectors proposed in (Bullo and Murray, 1999) and the properties of the Lie group $\text{SO}(3)$ in (Maithripala and Berg, 2015), an attitude error vector \mathbf{e}_R can be defined as the partial differential of φ with respect to \mathbf{R} , which are expressed as

$$\mathbf{e}_R(\mathbf{R}, \mathbf{R}_d) = \frac{\partial \varphi}{\partial \mathbf{R}} = \frac{1}{2\sqrt{1 + \text{tr}(\mathbf{R}_d^T \mathbf{R})}} (\mathbf{R}_d^T \mathbf{R} - \mathbf{R}^T \mathbf{R}_d)^\vee \quad (13)$$

where \mathbf{e}_R is the gradient of the error scalar function φ at its current attitude point \mathbf{R} . To make the denominator in (13) non-zero, the attitude error vector \mathbf{e}_R must be defined in the sublevel set $L = \{\mathbf{R} \in \text{SO}(3) | \varphi(\mathbf{R}, \mathbf{R}_d) < 2\}$.

Furthermore, according to the geometric description in (Maithripala and Berg, 2015) and using the left-invariant properties of Lie group, the velocity error vector \mathbf{e}_Ω can be defined as

$$\mathbf{e}_\Omega(\mathbf{R}(t), \mathbf{R}_d(t)) = (\mathbf{R}_e^T \dot{\mathbf{R}}_e)^\vee = \boldsymbol{\Omega} - \mathbf{R}^T \mathbf{R}_d \boldsymbol{\Omega}_d \quad (14)$$

Then, the time derivative of the error scalar function φ can be rewritten as the equation in (15),

which is similar to the properties and relationships between the location and velocity error vectors used in three-dimensional Euclid space.

$$\frac{d}{dt}\varphi(\mathbf{R}(t), \mathbf{R}_d(t)) = \mathbf{e}_R \cdot \mathbf{e}_\Omega \quad (15)$$

Notice that $\mathbf{e}_R, \mathbf{e}_\Omega \in \mathbb{R}^3$ do not live on the cotangent bundle $T_R^*\text{SO}(3)$ or the tangent bundle $T_R\text{SO}(3)$. Because the properties of the Lie group and Lie algebra are used here. The precise but complicated statement for the attitude and velocity error vectors are $\mathbf{R}\mathbf{e}_R^\wedge \in T_R^*\text{SO}(3)$ and $\mathbf{R}\mathbf{e}_\Omega^\wedge \in T_R\text{SO}(3)$ respectively (Bullo and Murray, 1999; Maithripala and Berg, 2015).

Furthermore, the attitude error dynamics are obtained as

$$\dot{\mathbf{e}}_R = \mathbf{E}\mathbf{e}_\Omega \quad (16)$$

$$\dot{\mathbf{e}}_\Omega = \mathbf{J}^{-1}(-\boldsymbol{\Omega} \times \mathbf{J}\boldsymbol{\Omega} + \mathbf{u} + \mathbf{d} + \mathbf{d}_0) - \boldsymbol{\alpha}_d \quad (17)$$

where $\mathbf{E} \in \mathbb{R}^{3 \times 3}$ and $\boldsymbol{\alpha}_d \in \mathbb{R}^3$ are given as

$$\mathbf{E} = \frac{1}{2\sqrt{1 + \text{tr}(\mathbf{R}_d^T \mathbf{R})}} (\text{tr}(\mathbf{R}^T \mathbf{R}_d) \mathbf{I} - \mathbf{R}^T \mathbf{R}_d + 2\mathbf{e}_R \mathbf{e}_R^T) \quad (18)$$

$$\boldsymbol{\alpha}_d = \mathbf{R}^T \mathbf{R}_d \dot{\boldsymbol{\Omega}}_d - \boldsymbol{\Omega}^\wedge \mathbf{R}^T \mathbf{R}_d \boldsymbol{\Omega}_d \quad (19)$$

It can be seen that \mathbf{E} is a variable matrix related to \mathbf{R}_e . In order to analysis the algebra properties of \mathbf{E} , we use the Rodrigues formula here as follows (Lee, 2012). For any $\mathbf{Q} \in L$, there exists a vector $\mathbf{x} \in \mathbb{R}^3$ with $\|\mathbf{x}\| \leq \pi$, such that

$$\mathbf{Q} = \exp(\mathbf{x}^\wedge) = \mathbf{I} + \frac{\sin\|\mathbf{x}\|}{\|\mathbf{x}\|} \mathbf{x}^\wedge + \frac{1 - \cos\|\mathbf{x}\|}{\|\mathbf{x}\|^2} (\mathbf{x}^\wedge)^2 \quad (20)$$

\mathbf{x} is the Rodrigues formula expression of $\mathbf{Q} \in L$

and satisfies $\|\mathbf{x}\| < \pi$. $\exp: \text{so}(3) \rightarrow \text{SO}(3)$ is the exponential map. The inverse of the exponential map can be defined as $\log: \text{SO}(3) \rightarrow \text{so}(3)$, which can be expressed by

$$\mathbf{x}^\wedge = \frac{\phi}{2 \sin \phi} (\mathbf{R} - \mathbf{R}^T) \quad (21)$$

where the variable ϕ is given by

$$\cos \phi = \frac{1}{2} [\text{tr}(\mathbf{R}) - 1], \quad \|\phi\| < \pi \quad (22)$$

With (20), the eigenvalues of matrix \mathbf{Q} can be calculated as

$$\lambda_Q^j = 1, \cos\|\mathbf{x}\| \pm \sin\|\mathbf{x}\|i, \quad j = 1, 2, 3 \quad (23)$$

Let $\mathbf{Q} = \mathbf{R}_e$ and substituting (20) and (23) into the formula of matrix \mathbf{E} in (18), we can also get that the eigenvalues of matrix \mathbf{E} are (Liu et al., 2016)

$$\lambda_E^j = \frac{1}{2} \cos \frac{\|\mathbf{x}\|}{2}, \frac{1}{2} \left(\cos \frac{\|\mathbf{x}\|}{2} \pm \sin \frac{\|\mathbf{x}\|}{2} i \right) \quad (24)$$

Furthermore, the determinant value of the matrix \mathbf{E} , are

$$\det(\mathbf{E}) = \prod_{j=1}^3 \lambda_E^j = \frac{1}{8} \cos \frac{\|\mathbf{x}\|}{2} \quad (25)$$

Since $\|\mathbf{x}\| < \pi$, it can be concluded that matrix \mathbf{E} is a positive definite and nonsingular matrix.

4 CONTROLLER DESIGN

This section mainly introduces a geometric adaptive robust sliding-mode attitude tracking controller on $\text{SO}(3)$. The control architecture is shown in Fig 1.

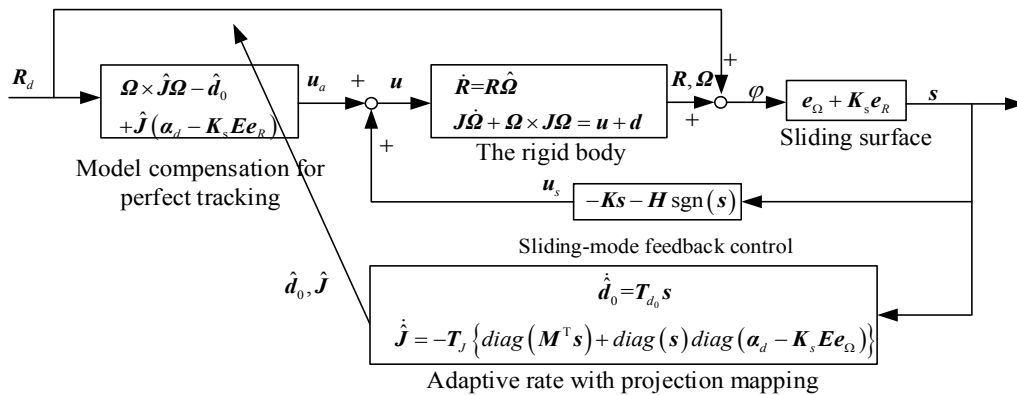


Figure 1: The structure of the proposed control system.

The controller mainly consists of two parts. The feedforward model compensation part which contains the adaption functions for the unknown parameters or slow-time-varying disturbance, and the variable structure feedback part. Both of them are designed based on the geometric sliding-mode surface \mathbf{s} . Therefore, we need to design a geometric asymptotically convergent sliding-mode surface firstly.

4.1 The Design of the Geometric Sliding-mode Surface

As the attitude vector \mathbf{e}_R and the velocity vector \mathbf{e}_Ω belong to the same space \mathbb{R}^3 , the vector operations, such as addition, subtraction and matrix multiplication, in Euclidean space can be used in this case. Then, the asymptotically convergent sliding-mode surface $\mathbf{s} = [s_1(t) \ s_2(t) \ s_3(t)]^T$ is introduced as

$$\mathbf{s} = \mathbf{e}_\Omega + \mathbf{K}_s \mathbf{e}_R \quad (26)$$

where $\mathbf{K}_s \in \mathbb{R}^{3 \times 3}$ is a constant positive definite diagonal matrix. The minimum eigenvalue of \mathbf{K}_s should be designed greater than or equal to $1/4$ and the reason will be detailed later in the stability analysis. \mathbf{K}_s decides the convergence speed of \mathbf{e}_R when the system reach on the sliding-mode surface $\mathbf{s} = \mathbf{0}$. Substituting (16) to (26), we can get that

$$\dot{\mathbf{e}}_R = -\mathbf{E} \mathbf{K}_s \mathbf{e}_R \quad (27)$$

Integrating it, we can get that

$$\mathbf{e}_R = \exp(\int -\mathbf{E} \mathbf{K}_s dt) \mathbf{e}_R(0) \quad (28)$$

Since matrix \mathbf{E} is positive definite. After the system reach on the sliding-mode surface $\mathbf{s} = \mathbf{0}$, the attitude tracking error \mathbf{e}_R will converge to its unique stable equilibrium $\|\mathbf{e}_R\| = 0$ exponentially.

4.2 Attitude Tracking Control

With the control architecture shown in Fig 1, the geometric adaptive robust sliding-mode attitude tracking control law \mathbf{u} consisting of the feedforward compensation part \mathbf{u}_a and the variable structure feedback part \mathbf{u}_s is shown as

$$\begin{cases} \mathbf{u} = \mathbf{u}_a + \mathbf{u}_s \\ \mathbf{u}_a = \boldsymbol{\Omega} \times \hat{\mathbf{J}} \boldsymbol{\Omega} - \hat{\mathbf{d}}_0 + \hat{\mathbf{J}} (\boldsymbol{\alpha}_d - \mathbf{K}_s \mathbf{E} \mathbf{e}_\Omega) \\ \mathbf{u}_s = -\mathbf{K} \mathbf{s} - \mathbf{H} \text{sgn}(\mathbf{s}) \end{cases} \quad (29)$$

where $\mathbf{K}, \mathbf{H} \in \mathbb{R}^{3 \times 3}$ are two constant positive definite diagonal matrix. The function $\text{sgn}(\mathbf{s})$ for the sliding-mode surfaces are defined as

$$\text{sgn}(\mathbf{s}) = [\text{sign}(s_1) \ \text{sign}(s_2) \ \text{sign}(s_3)]^T \quad (30)$$

where $\text{sign}(\cdot)$ is the sign function.

In (29), \mathbf{u}_a is designed for a feedforward compensation tracking through an online parameters adaptive law $\hat{\mathbf{J}}$ and $\hat{\mathbf{d}}_0$. $\hat{\mathbf{J}}$ and $\hat{\mathbf{d}}_0$ will be designed in the next subsection. \mathbf{u}_s is composed by a nominal stabilizing feedback $-\mathbf{K} \mathbf{s}$ and a robust feedback $-\mathbf{H} \text{sgn}(\mathbf{s})$. $\mathbf{K} \in \mathbb{R}^{3 \times 3}$ is a linear gain to determine the reaching law. $\mathbf{H} \in \mathbb{R}^{3 \times 3}$ is a parameter to determine the robustness of this system. The robustness is stronger with a larger \mathbf{H} . However, the inherent chattering phenomenon is more heavy with a larger \mathbf{H} . \mathbf{H} in this controller is designed as

$$\mathbf{H} = \mathbf{D}_1 \quad (31)$$

Remark 1: \mathbf{u}_a contains the estimated values of $\hat{\mathbf{d}}_0$ and $\hat{\mathbf{J}}$. Those model uncertainties and high-amplitude slow-time-varying disturbances can be estimated and compensated by this part. The low-amplitude high-frequency disturbances, which can not be estimated rapidly by the adaption functions, can be resolved by the variable structure part with a small switching term amplitude. The amplitude is determined by the upper bounds of the low-amplitude disturbance \mathbf{D}_1 . Therefore, the undesired chattering can be suppressed efficiently.

4.3 Adaptive Law Design with Projection Mapping and Rate Limits

In the feedforward compensation part \mathbf{u}_a , the diagonal matrix $\hat{\mathbf{J}}$ represents the estimated value of the rigid body's inertial matrix. $\hat{\mathbf{d}}_0$ represents the estimated value of the slow-time-varying disturbance. The update laws of those two parameters are designed as

$$\dot{\hat{\mathbf{d}}}_0 = \mathbf{T}_{d_0} \mathbf{s} \quad (32)$$

$$\dot{\hat{\mathbf{J}}} = -\mathbf{T}_J \left\{ \text{diag}(\mathbf{M}^T \mathbf{s}) + \text{diag}(\mathbf{s}) \text{diag}(\boldsymbol{\alpha}_d - \mathbf{K}_s \mathbf{E} \mathbf{e}_\Omega) \right\} \quad (33)$$

where $M \in \mathbb{R}^{3 \times 3}$ is given as

$$M = \begin{bmatrix} 0 & -\Omega_2\Omega_3 & \Omega_2\Omega_3 \\ \Omega_1\Omega_3 & 0 & -\Omega_1\Omega_3 \\ -\Omega_1\Omega_2 & \Omega_1\Omega_2 & 0 \end{bmatrix} \quad (34)$$

M satisfies the following equation

$$\Omega \times J\Omega = M \text{diag}(J) \quad (35)$$

$T_J, T_{d_0} \in \mathbb{R}^{3 \times 3}$ are two positive symmetric matrixes to accelerate or decelerate the adaption speed of \hat{J} and \hat{d}_0 .

In practice, J and d_0 are usually bounded. To avoid the oversize or undersize of the estimated values \hat{J} and \hat{d}_0 , a widely used projection map (Yao and Jiang, 2010; Yao et al., 2002) is used to keep the parameter estimates within a known bound, which is

$$\text{Proj}_{\hat{\theta}}(\zeta) = \begin{cases} \zeta, & \hat{\theta} \in \text{int}(\Omega_{\theta}) \text{ or } n_{\hat{\theta}}^T \zeta \leq 0 \\ (I - \frac{n_{\hat{\theta}} n_{\hat{\theta}}^T}{n_{\hat{\theta}}^T n_{\hat{\theta}}}) \zeta, & \hat{\theta} \in \Omega_{\theta} \text{ and } n_{\hat{\theta}}^T \zeta > 0 \end{cases} \quad (36)$$

where $\theta \in \mathbb{R}^m$ is the unknown parameter. $\hat{\theta}$ denotes the estimate value of θ . $\zeta \in \mathbb{R}^m$ is an adaptive law for θ . m is the dimension of θ . Ω_{θ} is the boundary of the unknown parameter θ , and $\text{int}(\Omega_{\theta})$ denotes the interior of this known boundary. $n_{\hat{\theta}}$ represents the outward unit normal vector at $\hat{\theta} \in \Omega_{\theta}$.

In order to limit the adaptive rate for the control process, a saturation function with a pre-set value $\dot{\theta}_M \in \mathbb{R}$ is defined as

$$\text{sat}_{\dot{\theta}_M}(\zeta) = \begin{cases} \zeta, & \|\zeta\| \leq \dot{\theta}_M \\ \frac{\dot{\theta}_M}{\|\zeta\|} \zeta, & \|\zeta\| > \dot{\theta}_M \end{cases} \quad (37)$$

The upper bound of the adaptive rate for J and d_0 are represented as $\dot{\theta}_J^M$ and $\dot{\theta}_{d_0}^M$, respectively.

Assuming that the uncertain estimate parameter $\hat{\theta}$ is updated using the projection mapping and the saturation function defined above in (36) and (37), the designed adaptive law can be modified as

$$\dot{\hat{\theta}} = \text{sat}_{\dot{\theta}_M}(\text{Proj}_{\hat{\theta}}(\tau)), \quad \hat{\theta}(0) \in \text{int} \Omega_{\theta} \quad (38)$$

where τ is the adaptive law proposed in (32) and

(33). According to (Yao and Tomizuka, 1996), the following properties for the function in (38) can be obtained as:

- i. The estimation values of J and d_0 are always within the known bounded set $\Omega_{\theta} \cup \text{int} \Omega_{\theta}$. Thus from assumption 1, $\theta < J_m \leq \hat{J} \leq J_M$ and $|\hat{d}_0| \leq D_0$ can be always satisfied.
- ii. The adaptive rate is uniformly bounded by $\forall t, \|\dot{\hat{\theta}}\| \leq \dot{\theta}_M$.
- iii. $(\hat{\theta} - \theta) \cdot (\text{Proj}_{\hat{\theta}}(\tau) - \tau) \leq 0, \forall \tau$.

4.4 Stability Analysis

The inertial matrix estimation error \tilde{J} and slow-time-varying disturbance estimation error \tilde{d}_0 are defined as

$$\begin{cases} \tilde{d}_0 = \hat{d}_0 - d_0 \\ \tilde{J} = \hat{J} - J \end{cases} \quad (39)$$

Theorem 1: With the control law (29), the adaption functions (32) and (33), the equilibrium point $(e_R, e_{\Omega}) = (\theta, \theta)$ of the tracking errors is almost global asymptotically stable, whose attraction region is given as (40) and (41). Moreover, the two estimation error \tilde{J} and \tilde{d}_0 are bounded.

$$\varphi(R(0), R_{\nu}(0)) < 2 \quad (40)$$

$$\begin{aligned} & \frac{1}{2} s(0) \cdot J s(0) + \frac{1}{2} \tilde{J}(0) \cdot T_J^{-1} \tilde{J}(0) \\ & + \frac{1}{2} \tilde{d}_0(0) \cdot T_{d_0}^{-1} \tilde{d}_0(0) < \lambda_{K_{\min}} (2 - \varphi(0)) \end{aligned} \quad (41)$$

where $\lambda_{K_{\min}}$ is the minimal eigenvalue of matrix K .

Proof: A positive semi-definite Lyapunov function candidate is constructed as follows

$$V = \frac{1}{2} s \cdot J s + \frac{1}{2} \tilde{J} \cdot T_J^{-1} \tilde{J} + \frac{1}{2} \tilde{d}_0 \cdot T_{d_0}^{-1} \tilde{d}_0 \quad (42)$$

where T_J, T_{d_0} are defined in (32) and (33), respectively. Compared with the dynamic characteristics of system, the time derivative of the slow-time-varying disturbance is small and close to zero. Then, differentiating the Lyapunov function gets that

$$\dot{V} = J s \cdot \dot{s} + \tilde{J} \cdot T_J^{-1} \dot{\tilde{J}} + \tilde{d}_0 \cdot T_{d_0}^{-1} \dot{\tilde{d}_0} \quad (43)$$

where the linear product “ \cdot ” for the vectors and the square matrixes are defined as (44), respectively.

$$\begin{cases} \mathbf{A} \cdot \mathbf{B} = \text{tr}(\mathbf{A}^T \mathbf{B}), & \mathbf{A} \in \mathbb{R}^{3 \times 3}, \mathbf{B} \in \mathbb{R}^{3 \times 3} \\ \mathbf{a} \cdot \mathbf{b} = \mathbf{a}^T \mathbf{b}, & \mathbf{a} \in \mathbb{R}^{3 \times 1}, \mathbf{b} \in \mathbb{R}^{3 \times 1} \end{cases} \quad (44)$$

The time derivative of the sliding-mode surface s is obtained as

$$\dot{s} = \mathbf{J}^{-1}(-\boldsymbol{\Omega} \times \mathbf{J}\boldsymbol{\Omega} + \mathbf{u} + \mathbf{d}_1 + \mathbf{d}_0) - \mathbf{a}_d + \mathbf{K}_s \mathbf{E} e_\Omega \quad (45)$$

Substituting (35), (44), (45) into (43), with the control law in (29) we can get

$$\begin{aligned} \dot{V} &= \mathbf{J} \cdot (\mathbf{J}^{-1}(-\boldsymbol{\Omega} \times \mathbf{J}\boldsymbol{\Omega} + \mathbf{u} + \mathbf{d}_1 + \mathbf{d}_0) - \mathbf{a}_d + \mathbf{K}_s \mathbf{E} e_\Omega) \\ &\quad + \tilde{\mathbf{J}} \cdot \mathbf{T}_J^{-1} \dot{\tilde{\mathbf{J}}} + \tilde{\mathbf{d}}_0 \cdot \mathbf{T}_{d_0}^{-1} \dot{\tilde{\mathbf{d}}}_0 \\ &= \mathbf{s} \cdot (-\mathbf{K}_s - \mathbf{H} \text{sgn}(\mathbf{s}) + \mathbf{M} \text{diag}(\tilde{\mathbf{J}}) + \tilde{\mathbf{J}}(\mathbf{a}_d - \mathbf{K}_s \mathbf{E} e_\Omega)) \\ &\quad + \tilde{\mathbf{J}} \cdot \mathbf{T}_J^{-1} \dot{\tilde{\mathbf{J}}} + \tilde{\mathbf{d}}_0 \cdot \mathbf{T}_{d_0}^{-1} \dot{\tilde{\mathbf{d}}}_0 + \mathbf{d}_1 - \tilde{\mathbf{d}}_0 \end{aligned} \quad (46)$$

Taking account of the adaptive law in (32-33) into (46), it holds

$$\begin{aligned} \dot{V} &\leq \mathbf{s} \cdot (-\mathbf{K}_s - \mathbf{H} \text{sgn}(\mathbf{s}) + \mathbf{d}_1) \\ &\leq -\mathbf{s} \cdot \mathbf{K}_s - \mathbf{H} \cdot |\mathbf{s}| + |\mathbf{d}_1| \cdot |\mathbf{s}| \end{aligned} \quad (47)$$

\mathbf{H} is designed in (31) with $\mathbf{H} = \mathbf{D}_1$. $|\mathbf{d}_1|$ is assumed to be bounded by \mathbf{D}_1 with $|\mathbf{d}_1| - \mathbf{H} \leq \mathbf{0}$ as shown in (9). Therefore the following inequality always holds

$$\dot{V} \leq -\mathbf{s} \cdot \mathbf{K}_s \leq 0 \quad (48)$$

If and only if $\|\mathbf{s}\|=0$, $\dot{V}=0$. With the Barbalat lemma, we can get $\|\mathbf{s}\| \rightarrow 0$ with $t \rightarrow \infty$. Moreover, when $\|\mathbf{s}\|=0$ is satisfied, the attitude tracking error \mathbf{e}_R will converge to its unique stable equilibrium $\|\mathbf{e}_R\|=0$ exponentially.

To make the denominator in (13) non-zero, the given condition $(\mathbf{R}(t), \mathbf{R}_d(t))$ should always lies in the sublevel set L . Therefore, (40) is proven. In order to prove (41), a new Lyapunov function is defined as

$$V_2 = V + \lambda_{K_{\min}} \varphi(\mathbf{R}, \mathbf{R}_d) \quad (49)$$

With the equations of (15) and (48), the time derivative of V_2 is formulated as

$$\begin{aligned} \dot{V}_2 &\leq -\mathbf{s} \cdot \mathbf{K}_s + \mathbf{e}_R \cdot \mathbf{K} \mathbf{e}_\Omega \\ &= -\left(\frac{2\mathbf{K}_s - \mathbf{I}}{2} \mathbf{e}_R + \mathbf{e}_\Omega\right) \cdot \mathbf{K} \left(\frac{2\mathbf{K}_s - \mathbf{I}}{2} \mathbf{e}_R + \mathbf{e}_\Omega\right) \\ &\quad - \mathbf{e}_R \cdot \left(\mathbf{K}_s - \frac{\mathbf{I}}{4}\right) \mathbf{e}_R \\ &\leq 0 \end{aligned} \quad (50)$$

\mathbf{K}_s is designed in (26). whose minimum eigenvalue is not smaller than $1/4$. Equation (50) implies that V_2 is non-increasing. Then, using (41), it holds that

$$\lambda_{K_{\min}} \varphi(\mathbf{R}, \mathbf{R}_d) \leq V_2(t) \leq V_2(0) < 2\lambda_{K_{\min}} \quad (51)$$

Therefore, $\varphi(\mathbf{R}, \mathbf{R}_d) < 2$ can be always hold. Then, (41) is proven.

The attraction region described by (40) and (41) almost covers SO(3) except a set of zero measure critical points where $\varphi(\mathbf{R}(0), \mathbf{R}_d(0))$ get its maximum value $\varphi(\mathbf{R}(0), \mathbf{R}_d(0)) = 2$. However, when the value of $\varphi(\mathbf{R}(0), \mathbf{R}_d(0))$ is closed to 2 and the norms of $\tilde{\mathbf{J}}(0)$ and $\tilde{\mathbf{d}}_0(0)$ are also large, the region of $\mathbf{e}_\Omega(0)$ calculated in (41) is small. However, we can adjust the controller parameters \mathbf{K} , \mathbf{T}_J and \mathbf{T}_{d_0} to enlarge the selection region of $\mathbf{e}_\Omega(0)$ such that (41) always holds.

As $\dot{V} \leq 0$ always hold, the Lyapunov function is bounded, which can prove that the estimate error $\tilde{\mathbf{J}}$ and $\tilde{\mathbf{d}}_0$ are bounded. However the estimate error may not converge to zero. From (32) and (33), it can be gotten that if $\|\mathbf{s}\| \rightarrow 0$, $\dot{\tilde{\mathbf{d}}}_0 \rightarrow \mathbf{0}$ and $\dot{\tilde{\mathbf{J}}} \rightarrow \mathbf{0}$. Therefore $\tilde{\mathbf{d}}_0$, $\tilde{\mathbf{J}}$ will not change at this time. Therefore, $\tilde{\mathbf{d}}_0$, $\tilde{\mathbf{J}}$ may not converge to zero. However the convergences of φ and $\|\mathbf{e}_R\|$ will not be influenced.

5 SIMULATION

In this section, the comparative simulations are carried out for the designed GARSMC, ARC, SMC, and the augmented PD controller designed in (Lee, 2012). A quadrotor UAV is used as an example.

The initial attitude is fixed as $\mathbf{R}(0) = \mathbf{I}$. The desired attitude trajectory $\mathbf{R}_d(t)$ is described using 3-2-1 Euler angles which is

$$\mathbf{R}_d(t) = \exp(\phi \mathbf{b}_x^\wedge) \exp(\theta \mathbf{b}_y^\wedge) \exp(\psi \mathbf{b}_z^\wedge).$$

\mathbf{b}_x , \mathbf{b}_y , \mathbf{b}_z are three axes of the rigid body. The Euler angles ϕ , θ , ψ represent roll, pitch and yaw angles, respectively, which are given as shown in Tab.1.

The information for the uncertain inertial matrix

and the external disturbances is setting as shown in Tab.2. The parameters used in the control law and the adaption function are given as shown in Tab.3.

Simulation results are presented in Figs 2-6.

Table 1: The desired Euler angles.

Euler angles	Values
Roll (rad)	$\phi(t) = \pi \sin(2t + 0.65\pi)$
Pitch (rad)	$\theta(t) = t + 0.02\pi$
Yaw (rad)	$\psi(t) = \pi \sin(3t - 0.65\pi)$

Table 3: Controller parameters.

Parameters	Values
Controller parameters	$K_s = \text{diag}(20 \ 20 \ 20)$ $K = \text{diag}(0.25 \ 0.25 \ 0.25)$
Amplification coefficient for the adaption function	$T_{d_0} = \text{diag}(3 \ 3 \ 3)$ $T_J = \text{diag}(1 \ 1 \ 1)$
Maximal adaptive law	$\dot{\theta}_{d_0}^M = 5$ $\dot{\theta}_J^M = 0.1$

In Fig 2, the responses of the proposed GARSMC are compared with those in ARC, SMC and geometric PD controller. It has been shown that the tracking errors φ and e_r of the geometric PD controller do not converge to zero with the influences of disturbances and parameter uncertainties. However, these characteristics are significantly improved by using the GARSMC. It also can be seen that the proposed

GARSMC has higher control accuracy than ARC. SMC has the same accuracy as the GARSMC. However, Fig 3 shows that there exists a heavy chattering in SMC. Even though, the saturation function is used to eliminate the undesired chattering. Therefore, the proposed GARSMC can achieve a high accuracy with a strong robustness, and it can also eliminate the chattering phenomenon efficiently.

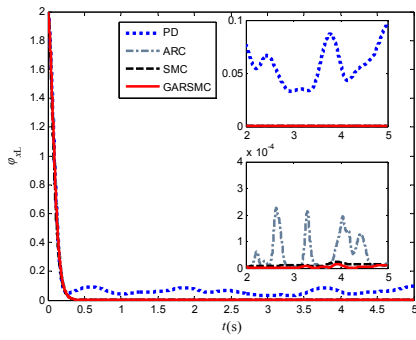
Fig 4 shows the history of the estimate values of the fixed disturbances d_0 and the inertial matrix J under the GARSMC. It can be observed that the inertial matrix and fixed disturbance will not converge to their true value. However, it can be shown in Fig 2 that the system stability and control precision are not influenced.

Fig 5 shows the information of the sliding-mode surface. It can be seen from Fig 5.(b) that the system will converge to the sliding-mode surface $s = 0$ firstly at $t = 0.22s$, and then converge to its stable point $e_r = 0$, $e_\Omega = 0$ along the sliding-mode surface $s = 0$. Fig 5.(b) shows that the inherent chattering phenomenon under the GARSMC is suppressed significantly compared with SMC.

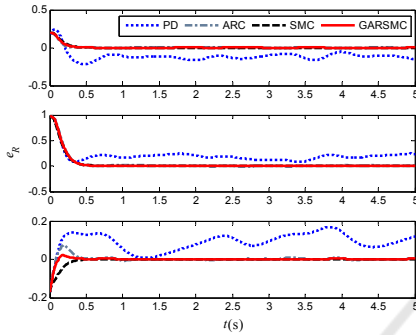
In order to illustrate the almost global convergence of the closed-loop system controlled by the GARSMC, the orientation maneuvers of spacecraft's body axes b_2 is depicted in Fig 6. The direction of rotation is marked with two red arrows. It can be seen that the closed-loop system controlled by the GARSMC can achieve the large-angle maneuver (greater than $\pi/2$ rad) without singularity and unwinding.

Table 2: Information for inertial matrix and disturbances.

	Inertial matrix ($\text{kg} \cdot \text{m}^2$)	Fixed disturbances ($\text{N} \cdot \text{m}$)	Time-varying disturbances ($\text{N} \cdot \text{m}$)
Real values	$J = \text{diag}(0.009 \ 0.009 \ 0.017)$	$d_0 = \begin{bmatrix} -0.8 \\ 0.8 \\ 0.5 \end{bmatrix}$	$d_1 = \begin{bmatrix} 0.25 \sin(0.5t) \\ -0.2 \sin(2t + 0.5\pi) \\ -0.15 \sin(t) \end{bmatrix}$
Initial estimated values	$\hat{J}(0) = \text{diag}(0.015 \ 0.015 \ 0.025)$	$\hat{d}_0(0) = \begin{bmatrix} 0 \\ 0 \\ 0 \end{bmatrix}$	--
Bounds	$J_m = \text{diag}(0.005 \ 0.005 \ 0.010)$ $J_M = \text{diag}(0.02 \ 0.02 \ 0.03)$	$D_0 = \begin{bmatrix} 1 \\ 1 \\ 1 \end{bmatrix}$	$D_1 = \begin{bmatrix} 0.3 \\ 0.3 \\ 0.3 \end{bmatrix}$



(a) Attitude error scalar function φ (rad)



(b) Attitude error vector e_R (rad)

Figure 2: Attitude tracking.

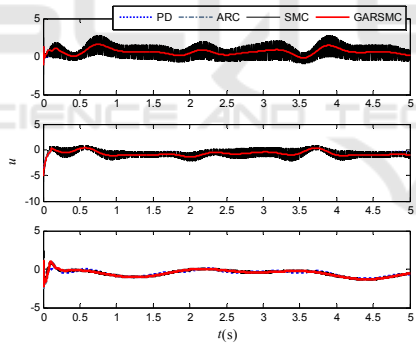
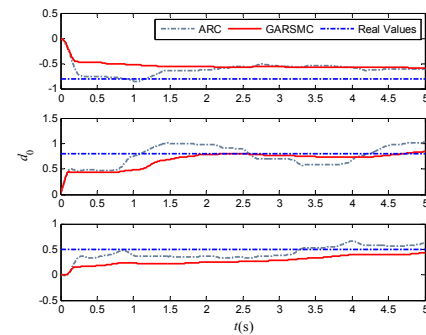
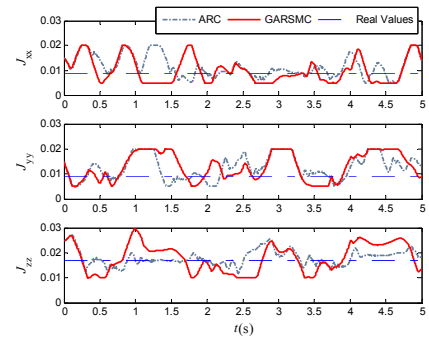


Figure 3: The control input (Nm).

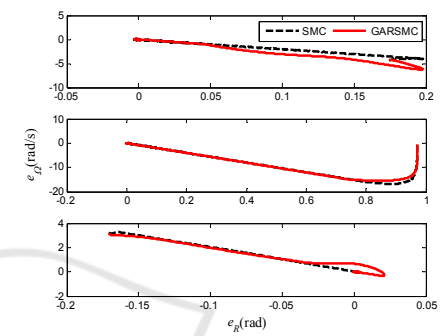


(a) Estimated fixed disturbances \hat{d}_0 (Nm)

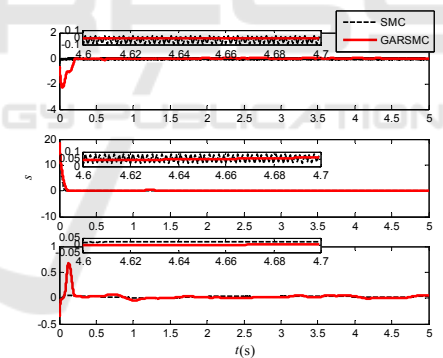


(b) Estimated inertial matrix \hat{J} (kg m²)

Figure 4: Estimate values of the parameters.



(a) Phase portrait



(b) Sliding-mode variables s (rad)

Figure 5: Sliding-mode surface.

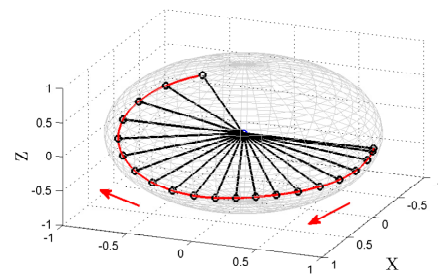


Figure 6: Orientation maneuver of b_2 .

6 CONCLUSIONS

This paper addresses the rigid-body attitude control modeled on the manifold $SO(3)$. This modeling scheme can avoid the singularities and ambiguities appearing in Euler angles and quaternion, respectively. The definitions and the algebra properties of the attitude error scalar function, attitude and velocity error vector on $SO(3)$ are introduced firstly. Then, a geometric asymptotical convergent sliding mode surface is designed based on these properties. Furthermore, a geometric adaptive robust sliding-mode attitude tracking controller system is developed to track the desired attitude command, considering the external interferences and model uncertainty. The values of the unknown inertial matrix and slow-time-varying disturbance are estimated online by the adaption functions. The fast-time-varying disturbance is dealt with by the variable structure part. Comparative simulation results demonstrate the high precision, strong robustness and little chattering of the proposed controller.

ACKNOWLEDGEMENTS

This work is supported by the National Natural Science Foundation (NNSF) of China under Grant 11572036.

REFERENCES

Bhat, S. P. & D. S. Bernstein (2000) A topological obstruction to continuous global stabilization of rotational motion and the unwinding phenomenon. *Systems & Control Letters*, 39, 63-70.

Boothby, W. M. 2003. An introduction to differentiable manifolds and Riemannian geometry. Amsterdam; New York: Academic Press.

Bullo, F. & A. D. Lewis. 2005. Geometric Control of Mechanical Systems. *Springer*.

Bullo, F. & R. M. Murray. 1995. Proportional Derivative (PD) Control on the Euclidean Group. In *European Control Conference*, 1091--1097.

Bullo, F. & R. M. Murray (1999) Tracking for fully actuated mechanical systems: a geometric framework. *Automatica*, 35, 17-34.

Fernando, T., J. Chandiramani, T. Lee & H. Gutierrez. 2011. Robust adaptive geometric tracking controls on $SO(3)$ with an application to the attitude dynamics of a quadrotor UAV. In *Decision and Control and European Control Conference*, 7380-7385.

Forbes, J. R. (2014) Passivity-Based Attitude Control on the Special Orthogonal Group of Rigid-Body Rotations.

Journal of Guidance Control & Dynamics, 36, 1596-1605.

Islam, S., P. X. Liu & A. E. Saddik (2017) Nonlinear robust adaptive sliding mode control design for miniature unmanned multirotor aerial vehicle. *International Journal of Control Automation & Systems*, 15, 1-8.

Koditschek, D. E. 1988. Application of a new Lyapunov function to global adaptive attitude tracking. In *Decision and Control*, 1988., *Proceedings of the IEEE Conference on*, 63-68 vol.1.

Lee, T. (2008) Computational geometric mechanics and control of rigid bodies. *Dissertations & Theses - Gradworks*.

Lee, T. (2012) Exponential stability of an attitude tracking control system on $SO(3)$ for large-angle rotational maneuvers ☆. *Systems & Control Letters*, 61, 231-237.

Lee, T., M. Leoky & N. H. McClamroch. 2011. Geometric tracking control of a quadrotor UAV on $SE(3)$. In *Decision and Control*, 5420-5425.

Liu, J. T., W. H. Wu, J. Li & Q. Xin (2016) Sliding mode variable structure attitude controller design of quadrotor UAVs on $SO(3)$.

Maithripala, D. H. S. & J. M. Berg. 2015. An intrinsic PID controller for mechanical systems on Lie groups. *Pergamon Press, Inc*.

Sanyal, A., A. Fosbury, N. Chaturvedi & D. S. Bernstein. 2009. Inertia-free spacecraft attitude trajectory tracking with internal-model-based disturbance rejection and almost global stabilization. In *Conference on American Control Conference*, 4830-4835.

Taeyoung, L. 2012. Robust global exponential attitude tracking controls on $SO(3)$. In *American Control Conference*, 2103-2108.

Yao, B., F. Bu, J. Reedy & T. C. Chiu (2002) Adaptive robust motion control of single-rod hydraulic actuators: theory and experiments. *IEEE/ASME Transactions on Mechatronics*, 5, 79-91.

Yao, B. & C. Jiang. 2010. Advanced motion control: From classical PID to nonlinear adaptive robust control. In *IEEE International Workshop on Advanced Motion Control*, 815-829.

Yao, B. & M. Tomizuka. 1996. Smooth robust adaptive sliding mode control of manipulators with guaranteed transient performance. In *American Control Conference*, 1176-1180 vol.1.

Zlotnik, D. E. & J. R. Forbes. 2014. Rotation-matrix-based attitude control without angular velocity measurements. In *American Control Conference*, 4931-4936.